Structural Monitoring and Maintenance, *Vol. 8, No. 2 (2021) 203-220*
DOI: https://doi.org/10.12989/smm.2021.8.2.203

Temperature monitoring and analysis of a long-span cable-stayed bridge during construction period

Xiudao Mei [1a], Yiyan Lu*[1] and Jing Shi [2b]

[1] *School of Civil Engineering, Wuhan University, 299 Bayi Road, Wuhan City, Hubei Province, China*
[2] *Department of Bridge Health Monitoring, State Key Laboratory for Health and Safety of Bridge Structures, 103 Jianshe Avenue, Wuhan City, Hubei Province, China*

(*Received March 11, 2021, Revised May 7, 2021, Accepted May 7, 2021*)

Abstract. The temperature induced response of long-span cable-stayed bridge in cantilever state is significant, which is of great interest to study the temperature characteristics during construction period. A method of analyzing the eigenvalue and its extremum of daily temperature based on cubic spline function (CSF) is proposed. By setting the fixed time interval reasonably, introducing variable time interval and extracting nodes at the MinMax of daily temperature, the obtained CSF can approach the measured temperature curve with high accuracy. Based on CSF, the temperature characteristics at three levels of measuring point, section and component are analyzed in turn. The temperature monitoring data of a cable-stayed bridge with main span of 938 m and side span of steel-concrete composited box girder (CBG) during construction are analyzed. The results show that the temperature variation of steel box girder is remarkable; the steel beam of CBG is similar to steel box girder before composited, and it turns stable after composited; the influence of PE color on cable temperature is notable than that of the cable specification; as blue PE cable, the temperature difference of cable vs pylon and cable vs CBG exceed 17°C and 13°C.

Keywords: cable-stayed bridge; temperature monitoring; construction period; cubic spline function; composite box girder; steel box girder

1. Introduction

Environmental conditions such as solar radiation induce variable temperature field in structure members through their layout and material thermal properties (Kelbek 1981), which is equivalent to apply a set of time-varying initial strain to the structure, changing the unstressed length and curvature of structure element (Yang *et al*. 2012), material elastic modulus (Yang *et al*. 2019), structural boundary conditions (Wang *et al*. 2018), resulting in time-varying static and dynamic response of the bridge structure (Montassar *et al*. 2015, Roberts *et al*. 2017). On the one hand, the temperature induced internal force is an important load (Guo *et al*. 2016), and the temperature effect in some bridge components even exceeds those by operating live load (Han *et al*. 2021); on the other hand, it is necessary to eliminate the temperature induced structural response before

*Corresponding author, Ph.D., Professor, E-mail: yylu901@163.com
[a] Ph.D., E-mail: biulmei@163.com
[b] Engineer, E-mail: shidajing@live.cn

Copyright © 2021 Techno-Press, Ltd.
http://www.techno-press.org/?journal=smm&subpage=7 ISSN: 2288-6605 (Print), 2288-6613 (Online)

condition assessment.

With the development of bridge health monitoring (BHM), many researches were carried out on structural temperature field and temperature induced effection (Abid *et al*. 2018, Farrar and Worden 2013, Kim 2017). Xu *et al*. (2010) studied ten-year monitoring data of Tsing Ma Bridge in the manner of equivalent temperature, bringing insight in the temperature characteristic of suspension bridge and the temperature induced response of structure displacement, maintaining the temperature sampling interval at 14.3 s. The temperature data of a steel box girder bridge were measured by Lee *et al*. (2016) for two years in a bridge specimen and the bridge in service nearby in order to calculate the effective temperature for thermal loads and the results were compared with Design Code. The impact of air temperature and solar radiation on temperature gradient distributions in concrete-encased composite girders was investigated by Abid *et al*. (2018), showing significant impact of the thickness of the girder's concrete members on temperature gradients and temperature distributions. Liu *et al*. (2019) investigated the vertical temperature gradient of composite girder of cable-stayed bridge with a main span of 560m based on the measured data and FEM analysis; it was found that the temperature gradient mode of the composite girder with no overhanging side girder was quite different from the standard form; the temperature sampling interval was 20 minutes. Tomé *et al*. (2018) used the thermal FEM to solve the two-dimensional temperature field of typical sections of a concrete cable-stayed bridge with a main span of 300 m and high piers; the equivalent temperature was used to formulate the structural temperature, and the sampling interval was 1 hour. Zhou *et al*. (2010) built an optimally back-propagation neural network (BPNN) to establish the relationship model between structural temperature and modal frequency. The average temperature, effective temperature and principal component temperature were used as input, and the measured modal frequency was taken as output to study the fitting effect of BPNN model. The analysis interval of temperature was 1 hour.

The above investigation claims importance of structural temperature for both bearing capacity evaluation and condition assessment. However, there are few research focus on temperature analysis of long-span cable-stayed bridge during construction stage. Actually, data acquisition and processing during construction period is more difficult than BHM during operation period for the following reasons. Firstly, wireless data transmission unit (DTU) (Harms *et al*. 2010) based on GPRS is often used. The poor 4G signal on the bridge site leads to weak DTU signal, discontinous data transmission and even packet loss (Liu *et al*. 2020). Secondly, frequent power failure during construction period cause data record interruption; the power failure may be external which spread to the whole construction site; more likely, it is the fault of certain power distribution cabinet which only affects certain sensors. Lastly, there are many outliers of monitored data due to the impact of large construction equipment on voltage in the power grid and fault of acquisition equipment. Observations show good quality of raw temperature data of SBG at night, while most of the abnormal values appear in the working hours. The above problems lead to both low quality and quantity of monitoring data for further data analysis, the data volume of some measuring points is only 1/3 of the expected one. A good data processing method should be able to make full use of the data mixed with missing and abnormal value.

According to the heat conduction equation, the temperature of a certain point in the structural temperature field has a continuous smooth solution, so a small amount of missing data can be filled by continuous function fitting. Although sinusoidal curves were used on certain conditions (Montassar *et al*. 2015, Xia *et al*. 2018), it is difficult to fit the daily structural temperature precisely by any single elementary function. Therefore, suitable fitting method is needed to extract the thermal characteristics and to integrate with other structural response parameters, such as the

correlation analysis between girder deflection and temperature.

The solution of the above problems depends on a targeted data processing method. The finite element method (FEM) uses shape function defined on single element to fit the whole physical field (Zienkiewicz *et al*. 2008). Bearing this idea in mind, this study uses cubic spline function (CSF) to fit daily structural temperature curve. The nodes of CSF are set by union of fixed time interval and variable time interval. In the following discussion, it can be seen that much fewer nodes than the raw data are needed for CSF, which can approach the original temperature curve precisely.

2. Methodology

2.1 CSF construction of origin measuring point

The objective of daily temperature curve fitting is to get the CSF with as few nodes as possible, and the fitting error should be less than 1°C. The specific time is converted into a real number, whose integer part represents the cumulative number of days since AD and the decimal part represents the very moment. The expression of CSF of daily temperature is shown in Eq. (1).

$$T = f(t), t \in [0,1] \tag{1}$$

2.1.1 Division of time interval

The method of combining fixed time interval (FTI) with variable time interval (VTI) is adopted. The so-called FTI is to divide 24 hours duration a day into n + 1 intervals, as shown in expression (2). The duration of the intervals is not fixed, which are shorter in the afternoon than in other time. The adjacent endpoints of each FTI coincide. In order to ensure the accuracy and completeness of temperature data within the first and the last FTI, the endpoints of the corresponding FTI can be moved forward one day or the next day for a certain time, such as 1 hour.

$$[0, t_{f1}] \cdots [t_{fi}, t_{f(i+1)}] \cdots [t_{fn}, 1], 0 < t_{fi} < 1 \tag{2}$$

The so-called VTI is to divide 24 hours a day into several intervals automatically, as shown in expression (3), according to the duration of missing data, which is determined by statistical results. The length of missing data affects the fitting error of CSF. When the temperature changes sharply, the missing time should be short, such as 1 hour; other periods are long, like two hours. The adjacent endpoints between VTI do not coincide. VTI is not considered when there is no missing data, which is the most common case in fact.

$$[0, t_{v1}] \cdots [t_{vi}, t_{v(i+1)}] \cdots [t_{vr}, 1], 0 < t_{vi} < 1 \tag{3}$$

The combination of FTI and VTI may produce some intervals with very short duration. When these very small intervals have contiguous adjacent interval at their endpoints, these cells are combined again; if not, the cells are discarded. The combined time intervals are shown in expression (4), and there are s + 1 intervals settled in total.

$$[0, t_{m1}] \cdots [t_{mi}, t_{m(i+1)}] \cdots [t_{ms}, 1], 0 < t_{mi} < 1 \tag{4}$$

FTI can ensure good approximation of the original data with a few nodes, and VTI can separate the missing data period. The combination of the two makes full use of temperature data with a small amount of data missing.

2.1.2 Elimination of abnormal value

The abnormal value refers to the prominent values mixed among the normal one but obviously deviated from the overall trend, which are handled in each interval of expression (4), and the following skills are mainly used. First, if the variance of all data in one interval is 0, this interval is discarded; that's to say, it is likely to be the fault of acquisition equipment if the temperature does not fluctuate for a long time. Second, the outlier elimination method based on temperature slope is adopted, which means that the temperature change per unit time cannot be too large. Last, cubic polynomial fitting is used within each interval, and the fitting error indicates outlier existence if it is greater than statistical value from normal data. After the outliers were rejected, cubic polynomial fitting is carried out again, and the vacancy caused by outliers are filled with fitting values.

2.1.3 Determination of nodes and boundary conditions

The cubic polynomial is used again on both endpoints and midpoint within each interval of expression (3) to get three node coordinates (t_i, T_i). The maximum temperature node and minimum temperature node in the day are acquired by traversing all s + 1 intervals. Then, the coordinates of all nodes are sorted in ascending order by time and the repeated nodes are eliminated. In addition, the temperature changing rate at moment 0 and 1 are calculated. So far, all the necessary conditions for CSF fitting including node coordinates and boundary conditions have been met.

2.1.4 Generation of CSF

Parameters of CSF are generated by using general algorithm and stored as cell array. Just only one cell array is needed for storing the CSF parameters of all original measuring point (OMP), where the row represents each day, and the column represents every single OMP.

2.2 CSF construction of virtual measuring point

Generated by linear combination of OMP, virtual measuring point (VMP) represents the temperature of structure component which can meet the requirement for structure analysis with FEM, data analysis, condition assessment, etc (Celik *et al*. 2018, Hall and McMullen 2004, Khaleghi *et al*. 2013). The generation of VMP is similar to the construction process of OMP. Firstly, the node coordinates are resampled according to the CSF of each OMP item; then these node coordinates are linearly combined to obtain node and boundary conditions; and finally, the CSF of VMP is fitted. According to the different data source and integration degree, there are first level virtual measuring point (VMP-I) and second level virtual measuring point (VMP-II).

2.2.1 VMP-I

VMP-I is defined within section of structure member, including the equivalent uniform temperature T_ε (Xu *et al*. 2010, Huang *et al*. 2018), and the equivalent gradient temperature T_κ (Tomé *et al*. 2018), as shown in Eqs. (5) and (6), where T represents the temperature field in cross-section, A is area of cross-section, y is the distance relative to centroid axis, I_c is moment

of inertia. T_κ is the temperature difference per unit length of cross-section, which can also be expressed by temperature difference on both sides of the section.

$$T_\varepsilon = \frac{1}{A} t dA \tag{5}$$

$$T_\kappa = \frac{1}{I_c} t y dA \tag{6}$$

The temperature field within section of bridge component is continuous, which can be equivalently equationed as follow based on finite discrete monitoring points.

$$T_\varepsilon = \sum_i T_i a_i, \quad \text{where} \quad a_i = \frac{A_i}{A} \tag{7}$$

$$T_\kappa = \sum_i T_i k_i, \quad \text{where} \quad k_i = \frac{y_i A_i}{I_c} \tag{8}$$

In Eqs. (7) and (8), A_i is the area represented by T_i of OMP *i*, y_i is the distance from OMP *i* to the centroid axis, a_i and k_i are linear combination coefficients, which are related to the location of OMP and section geometric properties. The combination coefficient should satisfy Eq. (9), which could be used for checking accuracy of the combination coefficients.

$$\sum_i a_i = 1; \quad \sum_i k_i = 0 \tag{9}$$

2.2.2 VMP-II

VMP-II is generated by linear combination of VMP-I and defined as synchronous temperature difference between structural components, such as cable *vs* girder and cable *vs* tower, in which only T_ε is considered.

2.3 Eigenvalue of daily temperature

The highest temperature T_H, lowest temperature T_L and temperature difference ΔT in a day are usually taken as eigenvalue to reflect the fluctuation of structural temperature, which are extracted from each measuring point by CSF, as shown in Eqs. (10)-(12).

$$T_H = \max\{f(t)\}, \quad t \in [0,1] \tag{10}$$

$$T_L = \min\{f(t)\}, \quad t \in [0,1] \tag{11}$$

$$\Delta T = T_H - T_L \tag{12}$$

In addition, the temperature change rate can reflect variation of ambient factors and the thermal properties of structural members, which can be derived from Eq. (1), see Eq. (13).

$$K = f'(t), t \in [0,1] \tag{13}$$

Similaly, the daily temperature eigenvalue of maximum heating rate K_H, maximum cooling rate K_L and changing rate difference ΔK can be obtained, as shown in Eq. (14)-(16).

$$K_H = \max\{f'(t)\}, \quad t \in [0,1] \tag{14}$$

$$K_L = \min\{f'(t)\}, \quad t \in [0,1] \tag{15}$$

$$\Delta K = K_H - K_L \tag{16}$$

2.4 Statistical characteristic of eigenvalue

The set of temperature eigenvalues of each measuring point during the whole construction period constitutes one sample, whose probability density function (PDF) p(x) is estimated by kernel smoothing function. PDF of eigenvalue can be used to understand the temperature distribution characteristics of the same measuring point and the comparison of different measuring points.

It is helpful to further investigate the thermal properties of bridge structure by studying the daily temperature time history under extreme weather condition. In this paper, the MinMax of measured samples is directly selected as extremum. The maximum value of T_H during the whole construction period is noted as $T_{H,max}$, the minimum value of T_L as $T_{L,min}$, and the maximum value of ΔT as ΔT_{max}.

2.5 Analysis flow chart

The main analysis process of temperature data is shown in Fig. 1, according to which the temperature characteristics of main girder, stay cable and pylon of a cable-stayed bridge during construction period are carried out. Obviously, the CSF construction becomes the keystone of the subsequent analysis.

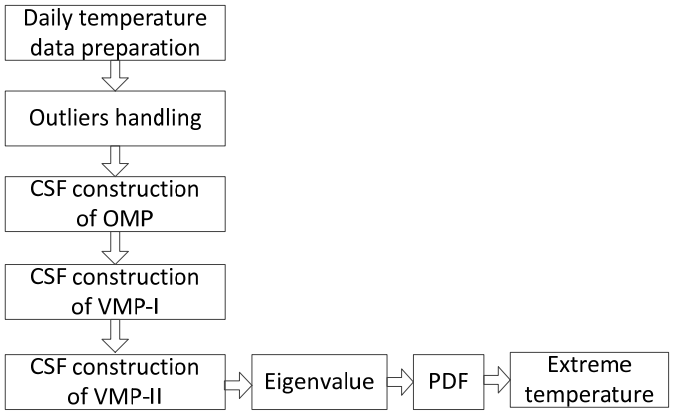

Fig. 1 Analysis flow chart

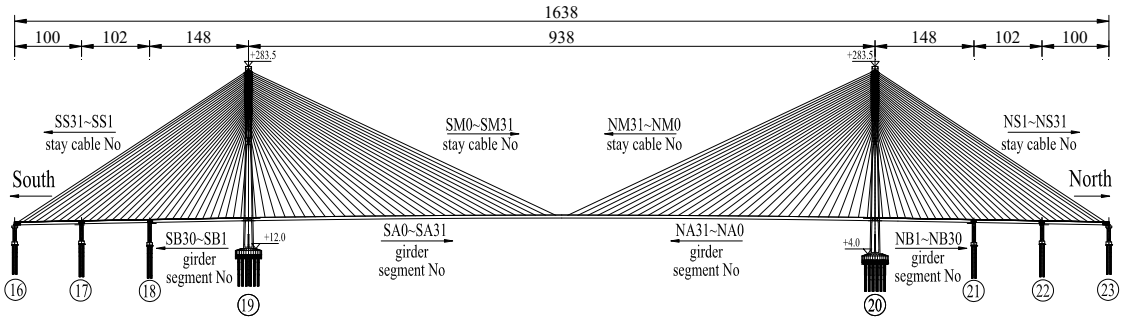

Fig. 2 Elevation layout of Wuhan Qingshan Yangtze River Bridge (unit: meter)

3. Engineering background and data source

3.1 Engineering background

Wuhan Qingshan Yangtze River Bridge is the passage across Yangtze River of the Fourth Ring Road in Wuhan City, China, whose main bridge is a cable-stayed bridge (Hu *et al*. 2018), as shown in Fig. 2, with steel box girder (SBG) in the mid span and steel-concrete composited box girder (CBG) in the side span. The azimuth of the bridge axis is 22° NBW. Wuhan Qingshan bridge has remarkable structural features such as long span (938 m), large girder width (10 lanes available), steel-concrete composited beam for side span and full floating structure system. Temperature monitoring during construction period helps to understand temperature induced response and improve the construction quality of the bridge structure. Based on the idea of life-cycle monitoring, an automatic monitoring system was gradually installed with the construction process. The sampled data were sent to the remote database by GPRS module. The sampling interval of temperature data was set as 1 minute.

3.2 Arrangement of measuring points

The arrangement of temperature measuring points of Qingshan Bridge is shown in Fig. 3. Fig. 3(a) shows the monitoring section of pylon, which is about 8.4 m above the bridge deck. Three measuring points are arranged in each pylon wall. The outer measuring points are 1 cm away from the surface, and the rest are 10 cm and 20 cm apart. Fig. 3(b) shows the section of steel girder of CBG (SG-CBG) with 14 measuring points evenly arranged, located in segment NB12. Fig. 3(c) shows the section of concrete slab of CBG (CS-CBG) with three measuring points right above the middle web. The top measuring point is 1cm away from the surface, and the rest are 5cm and 10cm apart. Fig. 3(d) displays the site photo about three temperature measuring cables, whose specification and PE sheath color are 127 wires in white (continued from other project), 187 wires in blue and 301 wires in blue, and their sectional arrangement of measuring points is shown in Fig. 3(e). Fig. 3(f) gives the section of SBG located in segment NA15 with 18 measuring points evenly arranged. There are 83 measuring points in total.

3.3 Data source

The work of temperature monitoring during the construction period of Wuhan Qingshan bridge

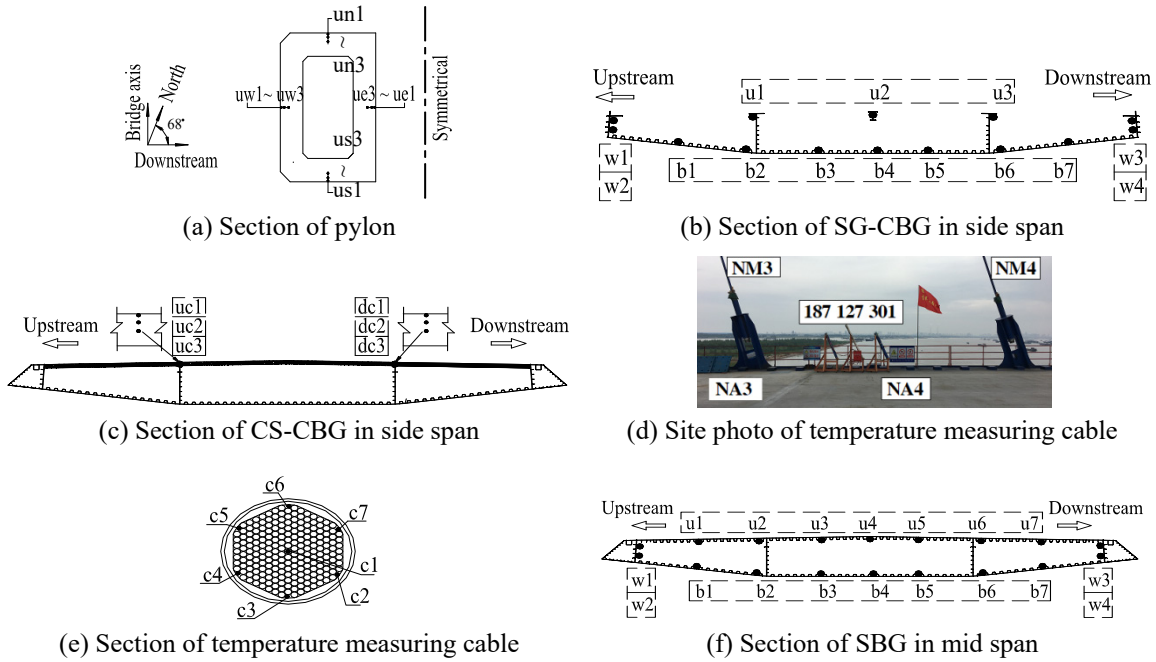

(a) Section of pylon

(b) Section of SG-CBG in side span

(c) Section of CS-CBG in side span

(d) Site photo of temperature measuring cable

(e) Section of temperature measuring cable

(f) Section of SBG in mid span

Fig. 3 Arrangement of temperature measuring points of Qingshan Bridge

is gradually carried out with the project promotion. The raw data of pylon, measuring cable, SG-CBG and CS-CBG were obtained in April 15, June 29, June 30 and September 20, 2018 respectively; and monitoring of SBG started from February 1, 2019. Several months after the closure of the main span, the construction power supply was interrupted, and all the monitoring above terminated in November 2019. The temperature data used in this paper came from these monitoring stages, during which time construction of the bridge deck pavement did not start.

4. Result

4.1 Temperature characteristic of OMP

4.1.1 SBG in mid span

The measuring points u2, w1 and b2 on different parts of SBG like the top plate, the side web plate and the bottom plate are taken respectively, their PDF of eigenvalues are shown in Fig. 4, their extreme temperature are listed in Table 1, while their extreme temperature changing rate is omitted. Both Fig. 4 and Table 1 reveal that in terms of temperature changing range and rate, the top plate proves to be the largest, the side web in the middle, and the bottom plate is the smallest. Actually, the top plate of SBG acts as the main path for heat exchange through directly affection by ambient factors such as solar radiation and rain fall, while these ambient factors are irrelevant to the bottom plate. As one of the main components bearing the cable force of stay cables, the side web plate is surrounded by steel plates from the wind fairing, the roof and the floor of SBG. The narrow space with dense steel plates arrangement tends to be affected by the complex temperature field of the surrounding steel plate, and the side web is thus affected.

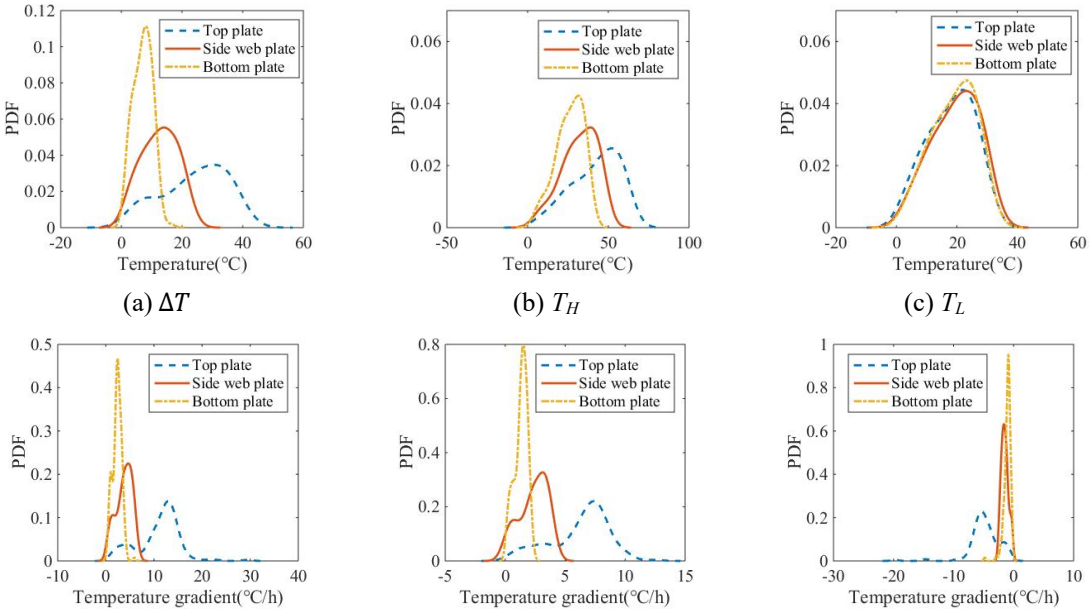

(a) ΔT (b) T_H (c) T_L

(d) ΔK (e) K_H (f) K_L

Fig. 4 PDF of eigenvalues of SBG

Table 1 Extreme temperature of SBG (unit: ℃)

Measuring points	ΔT_{max}	$T_{H,max}$	$T_{L,min}$
u2 (Top plate)	42.78	62.09	1.31
w1 (Side web plate)	24.10	49.09	1.92
b2 (Bottom plate)	16.29	39.31	2.54

The daily temperature curve of SBG when the extreme temperature happened is shown in Fig. 5, including the measured value and the fitting value by CSF. The ΔT_{max} of the top plate of SBG was 42.8°C, occured in May 22, 2019, with T_H equal to 57.3°C and T_L, equal to 14.5°C. It was in the early summer of Wuhan city, weather changed from cool night to sunny day resulting in obvious heating of SBG, as shown in Fig. 5(a). The ΔK_{max} of the top plate was 29.33°C/h, occured in July 31, 2019, with K_H equal to 9.6°C/h and K_L equal to -19.73°C/h. It was in midsummer, weather like sunny, cloudy and shower may appear alternately within the same day resulting in a complex temperature time history, as shown in Fig. 5(b). It can be seen that the fitting value of CSF is very close to the measured one.

4.1.2 Stay cable

Indigo-blue stay cable is the striking landscape of this bridge. Measuring point at the center wire of each cable are taken, their PDF of eigenvalues are shown in Fig. 6, their extreme temperatures are listed in Table 2, from which we can see that the color rather than the specification of PE sheath proves to be the main factor affecting thermal characteristic of stay cable. What's more, the thickness of PE sheath also affects the temperature changing rate. The PE

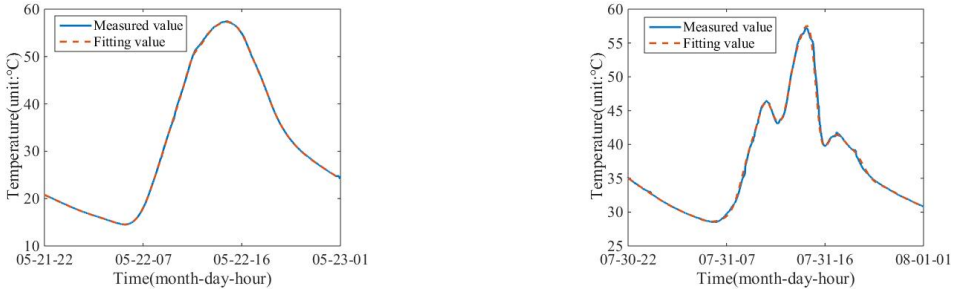

(a) ΔT_{max} (b) ΔK_{max}

Fig. 5 Daily temperature curves of SBG under extreme weather

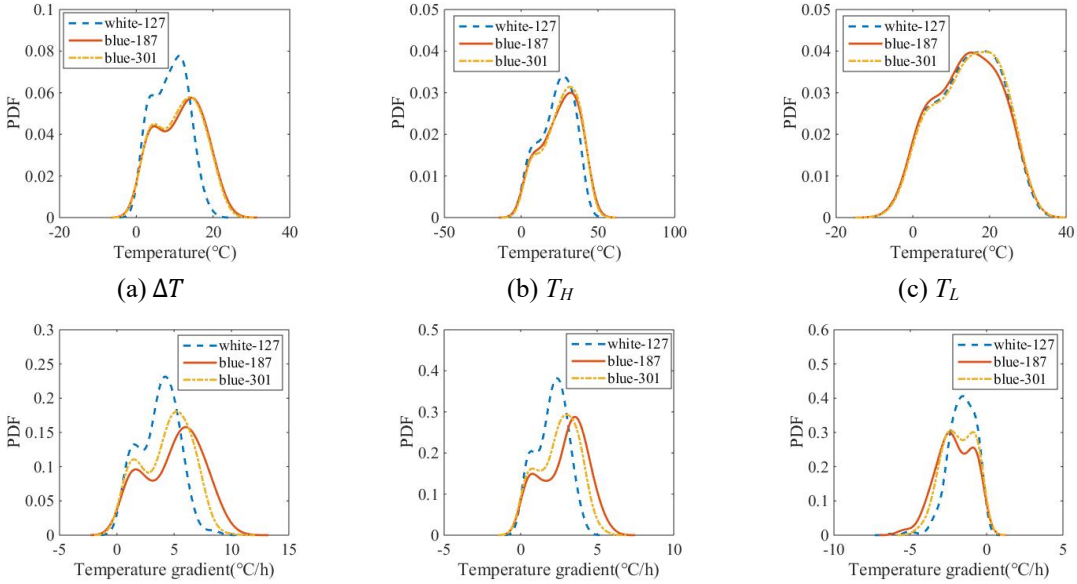

(a) ΔT (b) T_H (c) T_L

(d) ΔK (e) K_H (f) K_L

Fig. 6 PDF of eigenvalues measuring cable

Table 2 Extreme temperature of cable (unit: ℃)

Measuring cable	ΔT_{max}	$T_{H,max}$	$T_{L,min}$
white-127	19.10	41.84	-4.75
blue-187	23.93	46.85	-4.55
blue-301	23.27	47.53	-4.59

sheath thickness of blue-187 is 2 mm thinner than blue-301 resulting in more sensitive to temperature changing.

Fig. 7 shows the daily temperature curve of cable when the extreme temperature emerged. The ΔT_{max} of cable during construction period was 23.9℃, occurred in October 30, 2018, with T_H equal to 37.3℃ and T_L, equal to 13.4℃. It was in midautumn, with clear weather and major

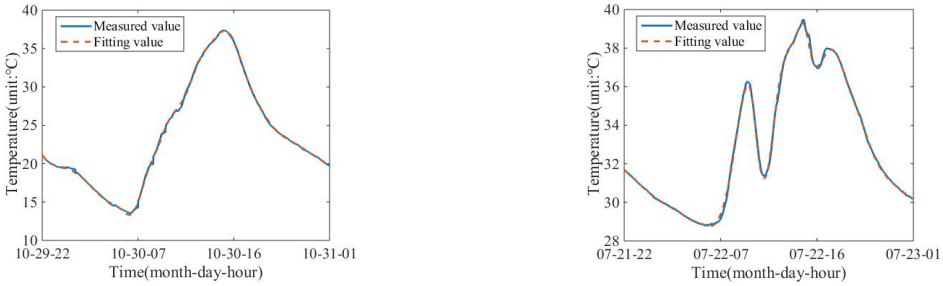

(a) ΔT_{max} (b) ΔK_{max}

Fig. 7 Daily temperature curves of cable under extreme weather

temperature difference between day and night, about 17°C in this day, as shown in Fig. 7(a). The ΔK_{max} of cable was 10.4°C/h, occurred in July 22, 2019, with K_H equal to 4.91°C/h and $K_{L,}$ equal to -5.49°C/h, as shown in Fig. 7(b). It was in midsummer, the same season of ΔK_{max} of SBG, while the amount of ΔK_{max} is about 1/3.6 of the latter, which due to the heat preservation effect of PE sheath. Again, the fitting value of CSF approach to the measured one very well.

4.1.3 CBG of side span

SG-CBG

Wuhan Qingshan bridge features steel-concrete composited beam. The measuring points u1, w1 and b2 on different parts of the SG-CBG like the top plate, the side web plate and the bottom plate are taken respectively, their PDF of eigenvalues are shown in Fig. 8. Since the period before composition is short, the PDF curve of ΔT extends widely with low probability.

Two daily temperature curves of the measuring points u1 on the top plate of SG-CBG under extreme temperature condition is shown in Fig. 9. The ΔT_{max} at the pure steel grider stage was 30.8°C, occurred in July 21, 2018, with T_H equal to 60.8°C and T_L equal to 30.0°C. The ΔT_{max} at the composited beam stage was 8.5°C, occurred in April 9, 2019, with T_H equal to 35.5°C and T_L equal to 27.0°C. Obviously, the daily temperature difference of top plate of SG-CBG becomes very small after composited.

The result of a further investigation on the temperature characteristic of SG-CBG after composited is shown in Table 3, from which comprehensive difference is found by comparing with the corresponding item in Table 1. The differences of both ΔT_{max} and $T_{H,max}$ claim the

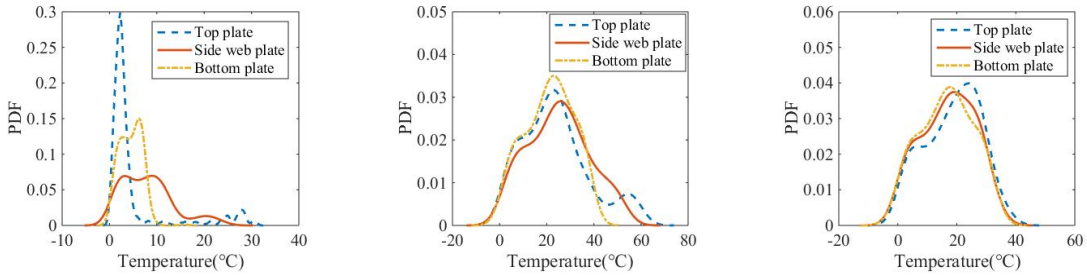

(a) ΔT (b) T_H (c) T_L

Fig. 8 PDF of eigenvalues of the SG-CBG

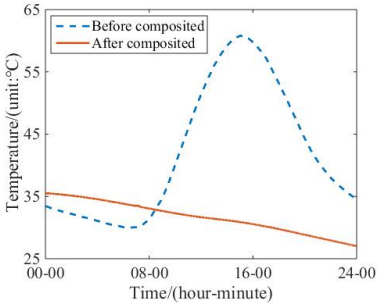

Fig. 9 Daily temperature curves of SG-CBG under extreme weather

Table 3 Extreme temperature of SG-CBG after composited (unit: ℃)

Measuring points	ΔT_{max}	$T_{H,max}$	$T_{L,min}$
u2 (Top plate)	8.49	40.14	-0.03
w1 (Side web plate)	14.60	43.23	-1.95
b2 (Bottom plate)	15.65	37.60	-2.39

diverse structural feature between CBG and SBG, while the difference of $T_{L,min}$, is related to the quantity of statistical samples. Temperature monitoring of SBG started too late to cover the complete winter.

CS-CBG

Taking the measuring points uc1, uc2, and uc3 as example, their PDF of eigenvalues of daily temperature are shown in Fig. 10, and the extreme temperature are listed in Table 4. It is obvious

Table 4 Extreme temperature of CS-CBG (unit: ℃)

Measuring points	ΔT_{max}	$T_{H,max}$	$T_{L,min}$
uc1 (Surface)	23.46	48.67	-1.90
uc2 (Middle)	14.78	42.62	-0.42
uc3 (Inner)	11.38	38.26	-0.27

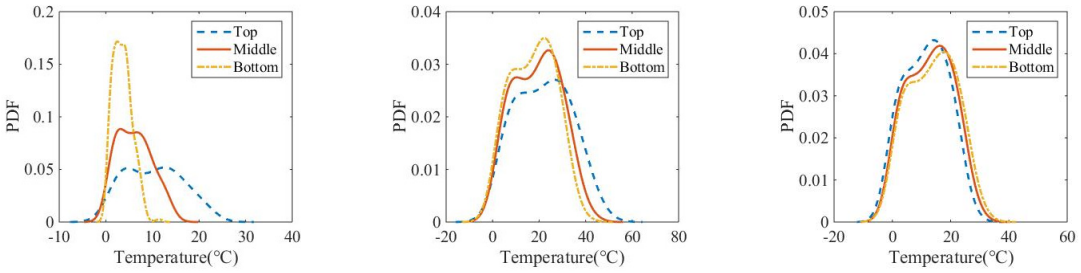

(a) ΔT (b) T_H (c) T_L

Fig. 10 PDF of eigenvalues of CS-CBG

Table 5 Extreme temperature of pylon (unit: ℃)

Measuring points	ΔT_{max}	$T_{H,max}$	$T_{L,min}$
uc1 (Surface)	14.81	41.75	-0.74
uc2 (Middle)	9.58	37.66	0.04
uc3 (Inner)	4.97	34.40	1.13

that as the measuring point going deeper, ΔT_{max} decreases rapidly, $\Delta T_{H,max}$ also decreases, while $\Delta T_{L,min}$ increases slightly.

4.1.4 Pylon

The PDF of eigenvalue is omitted for similarity to that of CS-CBG. The extreme temperature of measuring points on the west side wall of the upstream pylon column are listed in Table 5, showing a more stable temperature variation of the column than that of CS-CBG due to the much thicker wall, and the ΔT_{max} reach up to 5°C at the depth of 30 cm inside.

4.2 Temperature characteristic of VMP-I

According to the structural feature of Wuhan Qingshan Bridge, nine of VMP-I are set up as shown in Table 6. The top five are the equivalent uniform temperature T_{ε} and the last four are the equivalent gradient temperature T_k. T_k is defined as temperature difference over the opposite edge in corresponding direction of a section. Only the period after composited is concerned for both SG-CBG and CS-CBG. A wealth of temperature information on the structure section level of Wuhan Qingshan Bridge revealed by Table 6, just named a few. The temperature variation of SBG is the most active, followed by stay cable, and pylon comes the least. The variation of vertical temperature gradient of SBG (T_{ksv}) is much larger than that of horizontal direction (T_{ksh}), and both of them have negative values. The extreme value of the daily lowest temperature of vertical temperature difference of the pylon (T_{kpv}) is still positive, which is related to the azimuth of the bridge axis, temperature of the south side pylon wall is always higher than that of the north side.

Table 6 Extreme temperature of VMP-I (unit: ℃)

No.	Symbol	Parameter	ΔT_{max}	$T_{H,max}$	$T_{L,min}$
1	$T_{\varepsilon s}$	Axial of SBG	26.51	49.44	2.11
2	$T_{\varepsilon m}$	Axial of cable	23.94	46.85	-4.55
3	$T_{\varepsilon p}$	Axial of pylon	2.51	32.38	2.33
4	$T_{\varepsilon cs}$	Axial of SG-CBG	13.77	39.24	-1.77
5	$T_{\varepsilon cc}$	Axial of CS-CBG	12.25	39.27	0.01
6	T_{ksv}	Vertical of SBG	27.26	26.14	-2.32
7	T_{ksh}	Horizontal of SBG	5.29	4.45	-1.93
8	T_{kpv}	Vertical of pylon	2.51	5.88	0.83
9	T_{kph}	Horizontal of pylon	1.76	3.69	0.65

Table 7 Extreme temperature of VMP-II (unit: ℃)

No.	Parameter	ΔT_{max}	$T_{H,max}$	$T_{L,min}$
1	Cable vs SBG	11.55	5.58	-8.92
2	Cable vs SG-CBG	18.65	13.40	-9.65
3	Cable vs CS-CBG	19.23	13.19	-13.29
4	Cable vs pylon	22.08	17.03	-11.44
5	SBG vs pylon	25.02	20.56	-8.79

4.3 Temperature characteristic of VMP-II

The recommended value of temperature difference between structure components is given in the Chinese design specification of cable-stayed bridge (JTG/T 3365-01-2020, 2020), in which the temperature difference of cable vs steel girder is ±10℃, of cable vs concrete pylon is ±10~±15℃, lacking of consideration on concrete-steel composited beam and the color of PE sheath. The extreme temperature of VMP-II of Wuhan Qingshan Bridge are shown in Table 7. As blue PE sheathed stay cable, it can be seen that the value of the temperature difference of cable vs SBG is the smallest, the value of cable vs pylon exceeds the maximum recommended value, the value of both cable vs SG-CBG and cable vs CS-CBG approach the maximum value recommended. From the monitoring results of the white PE sheathed cable, the PE color of stay cable should be considered when determining relevant temperature difference.

5. Discussion

5.1 The setting of FTI

In order to approach the measured daily temperature curve with CSF precisely by less nodes, the key is to set up the FTI reasonably. The following techniques are used. Firstly, unequal spacing of node distribution is adopted, which is dense at noon and sparse at other times, as shown in expression (17). Secondly, the nodes at T_H and T_L are extracted for CSF to ensure the accuracy of eigenvalue of daily temperature. Finally, the midpoint of each interval is extracted as nodes. Under the above measures, 29 nodes are generated. After the VTI processing, the nodes number will change to 36 at most. There are 4 polynomial coefficients for each node of CSF, and there are 116~144 coefficients to be stored. When the sampling interval is 1 minute, there are 1440 pieces of raw data per day, which means about 90% of storage space can be saved and more space saved when the sampling interval is shorter. It can be seen from Figs. 5 and 7 that the fitted value by CSF can effectively approach to the measured value of complex time history curve, and the fitting error is less than 0.3°C.

$$[0,\ 0.1,\ 0.2,\ 0.3,\ 0.4,\ 0.4667,\ 0.5332,\ 0.6,\ 0.6664,\ 0.7333,\ 0.8,\ 0.9,\ 1] \quad (17)$$

5.2 The way for determination of extreme temperature

The cumulative distribution function (CDF) P(x) is obtained by integral of PDF, and the extreme temperature can be estimated theoretically according to CDF at a certain probability quantile, which is a common way for data analysis in BHM during operation period (Xu *et al*.

2021). The essence of kernel smoothing estimation method used to calculate PDF is weighted average method, with changing weight coefficients according to the density of sample points. However, the application of this method in construction stage implies the following problems. First of all, the number of eigenvalue samples is limited due to the short monitoring time and the missing of raw data, resulting in deviation of extreme value. Secondly, objectively asynchronous monitoring of structure components leads to uneven sample size which conceals dissimilar credibility among the extreme values. Finally, from the perspective of the whole bridge life, the extreme weather in a short construction period is improper to be called a small probability event; in other words, the MinMax is the extremum for the temperature population of construction period.

5.3 Arrangement of OMP on temperature induced structural response

VMP is deduced from OMP and can be used to study the temperature induced structural response. The girder of main span of Qingshan bridge was erected by single cantilever method, during which time the displacement of the cantilever frontend of girder and the deviation of the pylon top induced by temperature was concerned. Taking the structure under erecting of segment NA29 as an example, the sensitivity analysis of the above displacement to VMP-I in Table 6 is carried out, in which T_{ksh} of No. 7 and T_{kph} of No.9 are not considered, $T_{\varepsilon m}$ of No.2 is divided into $T_{\varepsilon mm}$ of the main span and $T_{\varepsilon ms}$ of the side span. Results are shown in Table 8. It can be seen that $T_{\varepsilon s}$ is the only notable factor on the displacement of mileage direction (DX) of cantilever frontend, while all VMP-I items have significant influence on the vertical displacement (DZ) of cantilever frontend. According to the measured value of ΔT_{max} in Table 6, the main influencing factors of DZ include $T_{\varepsilon mm}$ and $T_{\varepsilon ms}$ of stay cable, $T_{\varepsilon s}$ and T_{ksv} of SBG, followed by $T_{\varepsilon cs}$ and $T_{\varepsilon cc}$ of CBG. It is worth noting that the influence of T_{ksv} on DZ of the cantilever frontend is equivalent to that of $T_{\varepsilon s}$, while it is harder to obtain the former accurately based on temperature monitoring from the perspective of practice. The main influence factor of deviation of the pylon top (DX) is $T_{\varepsilon ms}$ of side span cable, with none of $T_{\varepsilon mm}$ of mid span cable.

The analysis above demonstrates the necessity of arrangement optimization of temperature measurement points for calculating the temperature induced response accurately, and the goal should be that VMP can represent the temperature distribution of structural components closely. The following improvements can be introduced. First, thermometric cables should also be

Table 8 Sensitivity analysis result (units: mm/°C)

No.	VMP-I	Cantilever frontend		Pylon top
		DX	DZ	DX
1	$T_{\varepsilon s}$	-3.4	9.2	0
2	$T_{\varepsilon mm}$	-0.1	-12	0
3	$T_{\varepsilon ms}$	-0.2	-10	-5.8
4	$T_{\varepsilon p}$	0.1	7.1	2.6
5	$T_{\varepsilon cs}$	0	3.1	1.7
6	$T_{\varepsilon cc}$	0	2.6	1.5
7	T_{ksv}	0.1	-7.7	-0.2
8	T_{kpv}	0.7	6.3	5.2

equipped with for the side span. Second, the monitoring of temperature gradient of SBG should be strengthened, and measuring points should be increased along the vertical direction of the section. Last, increase several measuring points in the wall thickness direction of pylon, and arrange a measuring point on the inner wall surface.

6. Conclusions

A method for fitting daily structural temperature with CSF is proposed, which is used to study the temperature features of Wuhan Qingshan bridge during construction period. Conclusions are summarized as follows.

(1) Through skills such as the reasonable setting of FTI, the adoption of VTI, the nodes at $\boldsymbol{T_H}$ and $\boldsymbol{T_L}$, the obtained CSF can well adapt to the temperature data with a small amount of missing and abnormal value monitored during construction period, and the fitting error is generally less than 0.3°C.
(2) Temperature variation of SBG is active, which is characterized by large daily temperature difference, high maximum daily temperature and remarkable vertical gradient. Temperature characteristic of SG-CBG before composited is similar to that of SBG, and it becomes stable after composited.
(3) The color of stay cable affects the temperature difference between cable and other components. For blue PE sheathed stay cable, the maximum temperature difference of cable vs pylon is 17°C; of cable vs CBG is more than 13°C, while of cable vs SBG is within 10°C.

Acknowledgments

The research described in this paper was financially supported by the Special Major Project of Technological Innovation of Hubei Province (2018AAA066) and the 2017 Sci-Tech Development Plan of China Railway Group Limited (2017-Key Project-37-01).

References

Abid, S.R., Mussa, F., Tayşi, N. and Özakça, M. (2018), "Experimental and finite element investigation of temperature distributions in concrete-encased steel girders", *Struct. Control Health Monitor.*, **25**(1), e2042. https://doi.org/10.1002/stc.2042

Celik, O., Terrell, T., Gul, M. and Catbas, F.N. (2018), "Sensor clustering technique for practical structural monitoring and maintenance", *Struct. Monitor. Maint., Int. J.*, **5**(2), 273-295. https://doi.org/10.12989/smm.2018.5.2.273

Farrar, C.R. and Worden, K. (2013), *Structural Health Monitoring: A Machine Learning Perspective*, A John Wiley and Sons, Ltd., Publication, Chichester, West Sussex, UK.

Guo, J., Zhong, J., Dang, X. and Yuan, W. (2016), "Seismic responses of a cable-stayed bridge with consideration of uniform temperature load", *Appl. Sci.-Basel*, **6**(12), 408. https://doi.org/10.3390/app6120408.

Hall, D.L. and McMullen, S.A. (2004), *Mathematical Techniques In Multisensor Data Fusion* (Second Edition), Artech House, London, England, UK.

Han, Q., Ma, Q., Xu, J. and Liu, M. (2021), "Structural health monitoring research under varying

temperature condition: A review", *J. Civil Struct. Health Monitor.*, **11**(1), 149-173. https://doi.org/10.1007/s13349-020-00444-x.

Harms, T., Sedigh, S. and Bastianini, F. (2010), "Structural health monitoring of bridges using wireless sensor networks", *IEEE Instrumentation and Measurement Magazine*, **13**(6), 14-18. https://doi.org/10.1109/MIM.2010.5669608

Hu, H.Y., Xu, G.Y. and Zhang, Y.F. (2018), "Key techniques for design of main girder of main bridge of wuhan qingshan changjiang river highway bridge", *Bridge Constr.*, **48**(5), 81-85.

Huang, H.B., Yi, T.H., Li, H.N. and Liu, H. (2018), "New representative temperature for performance alarming of bridge expansion joints through temperature-displacement relationship", *J. Bridge Eng.*, **23**(7), 04018043. https://doi.org/ 10.1061/(ASCE)BE.1943-5592.0001258

Kelbek (1981), Influence of Solar Radiation On Bridge Structure, China Railway Publishing House, Beijing, China.

Khaleghi, B., Khamis, A., Karray, F.O. and Razavi, S.N. (2013), "Multisensor data fusion: A review of the state-of-the-art", *Inform. Fusion*, **14**(1), 28-44. https://doi.org/ 10.1016/j.inffus.2011.08.001

Kim, H.J. (2017), "Analysis of variation rate of displacement to temperature of service stage Cable-Stayed bridge using temperatures and displacement data", In: Caicedo J., Pakzad S. (eds), *Dynamics of Civil Structures*, *Volume 2. Conference Proceedings of the Society for Experimental Mechanics Series*. https://doi.org/10.1007/978-3-319-54777-0_3

Lee, S.H., Shin, H.K., Kim, K.N. and Jung, K.S. (2016), "An experimental study for estimation of effective temperature for design in steel box girder bridge", *J. Korean Soc. Steel Constr.*, **28**(6), 449-458. https://doi.org/10.7781/KJOSS.2016.28.6.449

Liu, J., Liu, Y., Jiang, L. and Zhang, N. (2019), "Long-term field test of temperature gradients on the composite girder of a long-span cable-stayed bridge", *Adv. Struct. Eng.*, **22**(13), 2785-2798. https://doi.org/10.1177/1369433219851300

Liu, H., Ding, Y.L., Zhao, H.W., Wang, M.Y. and Geng, F.F. (2020), "Deep learning-based recovery method for missing structural temperature data using LSTM network", *Struct. Monitor. Maint., Int. J.*, **7**(2), 109-124. https://doi.org/10.12989/smm.2020.7.2.109

Maleki, S. and Maghsoudi-Barmi, A. (2016), "Effects of concurrent earthquake and temperature loadings on cable-Stayed bridges", *Int. J. Struct. Stabil. Dyn.*, **16**(06), 155002. https://doi.org/10.1142/S0219455415500200

Ministry of Transport of the People's Republic of China (2020), Specifications for Design of Highway Cable-stayed Bridge, JTG/T 3365-01-2020; Beijing, China.

Montassar, S., Mekki, O.B. and Vairo, G. (2015), "On the effects of uniform temperature variations on stay cables", *J. Civil Struct. Health Monitor.*, **5**(5), 735-742. https://doi.org/ 10.1007/s13349-015-0140-9

Roberts, G.W., Brown, C.J. and Tang, X. (2017), "Correlated GNSS and temperature measurements at 10-minute intervals on the Severn Suspension Bridge", *Appl. Geomat.*, **9**(2), 115-124. https://doi.org/ 10.1007/s12518-017-0187-x

Tomé, S.E., Pimentel, M. and Figueiras, J. (2018), "Structural response of a concrete cable-stayed bridge under thermal loads", *Eng. Struct.*, **176**(C), 652-672. https://doi.org/ 10.1016/j.engstruct.2018.09.029

Wang, Z.C., Zha, G.P., Ren, W.X., Hu, K. and Yang, H. (2018), "Nonlinear boundary parameter identification of bridges based on temperature-induced strains", *Struct. Eng. Mech., Int. J.*, **68**(5), 563-573. https://doi.org/10.12989/sem.2018.68.5.563

Xia, Q., Zhou, L.M. and Zhang, J. (2018), "Thermal performance analysis of a long-span suspension bridge with long-term monitoring data", *J. Civil Struct. Health Monitor.*, **8**(4), 543-553. https://doi.org/ 10.1007/s13349-018-0299-y

Xu, Y.L., Chen, B., Ng, C.L., Wong, K.Y. and Chan, W.Y. (2010), "Monitoring temperature effect on a long suspension bridge", *Struct. Control Health Monitor.*, **17**(6), 632-653. https://doi.org/ 10.1002/stc.340

Xu, X., Xu, Y.L., Ren, Y. and Huang, Q. (2021), "Site-specific extreme load estimation of a long-span cable-stayed bridge", *J. Bridge Eng.*, **26**(4), 05021001. https://doi.org/10.1061/(ASCE)BE.1943-5592.0001700

Yang, J.H., Im, D.K., Kim, C.H., Ahn, S.S. and Lee, W.S. (2012), "Construction and geometry control of

Incheon cable-stayed bridge", *Struct. Eng. Int.*, **22**(1), 49-52. https://doi.org/10.2749/101686612X13216060213310

Yang, S., Liu, B., Li, Y. and Zhang, M. (2019), "Effects of environmental temperature and age on the elastic modulus of concrete", *Struct. Eng. Mech., Int. J.*, **72**(6), 737-746. https://doi.org/10.12989/sem.2019.72.6.737

Zhou, H.F., Ni, Y.Q. and Ko, J.M. (2010), "Constructing input to neural networks for modeling temperature-caused modal variability: Mean temperatures, effective temperatures, and principal components of temperatures", *Eng. Struct.*, **32**(6), 1747-1759. https://doi.org/10.1016/j.engstruct.2010.02.026

Zhou, L., Chen, L., Xia, Y. and Koo, K.Y. (2020), "Temperature-induced structural static responses of a long-span steel box girder suspension bridge", *J. Zhejiang University-Science A*, **21**(7), 580-592. https://doi.org/ 10.1631/jzus.A1900490

Zienkiewicz, O.C., Taylor, R.L. and Zhu, J.Z. (2008), *The Finite Element Method*: *Its Basis and Fundamentals*, (6th edition), Elsevier (Singapore) Pte Ltd, Singapore.

TY